JGR Atmospheres

RESEARCH ARTICLE
10.1029/2019JD031997

Surface Expressions of Atmospheric Thermal Tides in the Tropical Atlantic and Their Impact on Open-Ocean Precipitation

J. A. Christophersen[1], G. R. Foltz[2], and R. C. Perez[2]

[1]National Research Council, Naval Research Laboratory, Monterey, CA, USA, [2]NOAA/Atlantic Oceanographic and Meteorological Laboratory/Physical Oceanography Division, Miami, FL, USA

Key Points:
- MERRA-2 represents well the diurnal cycles of surface pressure and winds, and hence atmospheric thermal tides in the tropical Atlantic
- Nonmigrating atmospheric thermal tides are largely responsible for diurnal cycles of meridional wind anomalies in the tropical Atlantic
- Diurnal cycles in divergence/convergence and precipitation in the Atlantic Ocean may be related to diurnal cycles of convection over Africa

Correspondence to:
J. A. Christophersen,
jonathan.christophersen.ctr@nrlmry.navy.mil

Citation:
Christophersen, J. A., Foltz, G. R., & Perez, R. C. (2020). Surface expressions of atmospheric thermal tides in the tropical Atlantic and their impact on open-ocean precipitation. *Journal of Geophysical Research: Atmospheres*, *125*, e2019JD031997. https://doi.org/10.1029/2019JD031997

Received 5 NOV 2019
Accepted 19 SEP 2020
Accepted article online 30 OCT 2020

Abstract Diurnal and semidiurnal variations of atmospheric pressure and surface winds are fundamental to the Earth-Sun system. Past research in the tropical Pacific shows semidiurnal and diurnal patterns in the zonal and meridional wind anomalies, respectively. While the semidiurnal zonal wind pattern is consistent with atmospheric thermal tidal forcing, it is not yet certain what drives diurnal meridional wind variability. This study examines the diurnal cycle of meridional winds in the tropical Atlantic Ocean across four different seasons and the extent to which they impact the diurnal evolution of open-ocean precipitation in boreal summer. Comparisons of direct observations from long-term moored buoys to an atmospheric reanalysis (MERRA-2) show that MERRA-2 reproduces diurnal and semidiurnal pressure and wind variations. The MERRA-2 atmospheric thermal tides are decomposed into migrating and nonmigrating tidal components, and the linear terms in the zonal and meridional momentum equations are calculated. There is an approximate balance between the acceleration and pressure gradient terms for the zonal migrating momentum budget in the open ocean, with larger residuals or imbalances between those terms for the other budgets. The meridional nonmigrating budget shows largest residuals near the African coastline, indicating that nonlinear processes like the evening initiation of convection are important over land. This evening convection drives the meridional component of surface convergence which is translated offshore by the nonmigrating tide in the form of gravity waves, potentially modified by the African Easterly Jet. During boreal summer, this convergence helps to induce a morning peak of precipitation over the open ocean.

Plain Language Summary The Sun's radiation is absorbed by different chemicals (ozone and water vapor) in the atmosphere, to which the surface atmosphere response can be observed as a wave-like pattern that migrates westward in pressure data. East-west wind patterns are explained as atmospheric thermal tides forced by the solar radiation in the tropical Atlantic that migrate westward around globe twice per day. We examine the cause of the diurnal north-south wind velocity variations, which had yet to be fully explained, and how they influence rainfall over the open-ocean. Nonmigrating (no westward movement) atmospheric tides drive the north-south wind pattern, carrying with them a signal of low-level convergence of the wind from western Africa to the middle of the tropical Atlantic Ocean, which helps to initiate early morning rainfall during the boreal summer. Climate models are deficient at simulating diurnal rainfall, and these results may aid in improving model precipitation.

1. Introduction

Atmospheric thermal tides, composed of migrating and nonmigrating portions, are fundamental modes of global diurnal variability that are caused by thermally excited oscillations. Chapman and Lindzen (1970) point out that the equations governing atmospheric tides (Laplace's tidal equation) can be solved analytically using a simple temperature profile. Solar absorption by ozone in the stratosphere contributes to roughly two thirds of the observed magnitude of the semidiurnal migrating tide in the tropics, while the other one third is explained by solar absorption by water vapor (Butler & Small, 1963; Chapman & Lindzen, 1970; Sakazaki & Hamilton, 2017). The diurnal nonmigrating tide is fueled by the release of latent heat due to tropical convection (Sakazaki et al., 2015) or other zonal inhomogeneities (e.g., land-ocean temperature difference and topography) (Dai & Wang, 1999; Sakazaki & Hamilton, 2017).

At the surface, these global-scale waves have periods that are integral fractions of a solar day (Chapman & Lindzen, 1970; Dai & Wang, 1999; Hagan & Robel, 2001) with the migrating component exhibiting a semidiurnal (12-hr) period and nonmigrating manifesting as a diurnal variation (Chapman & Lindzen, 1970). The response to atmospheric heating and vertical eddy conduction of heat (i.e., the transfer of heat by eddies) at the surface is internal gravity waves that propagate vertically from the Earth's surface and increase in amplitude with height (Chapman & Lindzen, 1970; Dai & Wang, 1999). The waves cause fluctuations in pressure, temperature, and winds from the surface to the thermosphere and are referred to as atmospheric thermal tides (ATTs; Chapman & Lindzen, 1970; Dai & Wang, 1999; Haurwitz & Cowley, 1973; Hsu & Hoskins, 1989; Wallace & Hartranft, 1969).

Maximum tidal amplitudes are reached in the mesosphere and lower thermosphere region (Chapman & Lindzen, 1970; Lu et al., 2012), motivating most previous studies to concentrate on this region (Hagan & Forbes, 2003; Lu et al., 2012). Previous studies on the observed surface response to ATTs have focused on diurnal and semidiurnal surface oscillations over the tropical Pacific Ocean, far away from the influence of land, primarily using annual composites (e.g., Dai & Deser, 1999; Dai & Wang, 1999; Deser, 1994; Deser & Smith, 1998; Ueyama & Deser, 2008). This study extends previous work to the tropical Atlantic while also investigating seasonality and the effects of land-ocean interaction.

Due to the zonal homogeneity of ozone in the stratosphere, solar absorption in this region produces a migrating tide that propagates westward with the apparent motion of the Sun. This semidiurnal tide (S_2) is thought to be the dominant signal over the globe and has a regularly distributed atmospheric pressure amplitude of ~1 mb in the tropics, with maxima at 9:00–10:00 and 19:00–20:00 local time (Dai & Wang, 1999). The dominance of the semidiurnal harmonic is due to vertically trapped diurnal modes associated with stratospheric heating (Chapman & Lindzen, 1970; Covey et al., 2011). Using the Tropical Atmosphere-Ocean (TAO) moored buoys in the Pacific Ocean, Ueyama and Deser (2008) (hereafter UD08) and Deser and Smith (1998) (referred to as DS98) showed evidence that the semidiurnal pressure wave from migrating atmospheric tides is associated with a semidiurnal near-surface zonal wind anomaly pattern over the open ocean. These results helped broaden our understanding of the diurnal evolution of the divergence field and convective rainfall in the tropics.

In contrast, the nonmigrating component of the ATT is not Sun-synchronous, is highly dependent on longitude and latitude, and is associated with diurnal oscillations (S_1) over the globe. While the semidiurnal migrating tide has been shown to be generally larger in amplitude than the diurnal nonmigrating tide, studies have also found the nonmigrating component to be equally important in some regions over the tropical Pacific (UD08). UD08 suggested that nonmigrating tides may play a role in diurnal variations of the meridional winds in the tropical Pacific. However, a direct mechanism to explain this linkage has not yet been established. It is important to understand this connection, as the diurnal cycle of the meridional winds is considered to be important for explaining the diurnal evolution of precipitation over the tropical Pacific Ocean (UD08), and this may hold across all of the tropical oceans.

It is well established that rainfall over continental regions in the tropics occurs during the late-afternoon and early-evening hours due to the diurnal initiation of convection driven by land surface heating (Garreaud & Wallace, 1997; Hamilton, 1981; Hendon & Woodberry, 1993; Kousky, 1980). Precipitation over the open ocean has an observed maximum during early-morning hours. This could be due either to radiative cooling in cloud tops (Kraus, 1963; Lavoie, 1963; Sui et al., 1998; Tao et al., 1996) or dynamic radiation-convection, which is driven by day-night differences in radiative cooling (Gray & Jacobson, 1977). However, it is possible other factors could contribute to the observed early-morning maximum. While the diurnal cycle of precipitation has been well resolved by observations over continental regions, open-ocean precipitation is still relatively understudied due to limited rainfall measurements away from land. Bain et al. (2010) discussed the diurnal cycle of open-ocean cloudiness in the Intertropical Convergence Zone (ITCZ) located in the eastern tropical Pacific and found peaks of cold infrared radiation (high cloud tops) during the morning (06:00–09:00 LT) and in the afternoon (13:00–16:00 LT).

Further motivation for this study comes from the difficulty that many atmospheric and coupled ocean-atmosphere models have in realistically simulating clouds and precipitation (Dai, 2006). On diurnal time scales, during the warm season (austral summer for the southern hemisphere and boreal summer for Northern Hemisphere) convective initiation typically begins too early in the day in tropical continental regions in

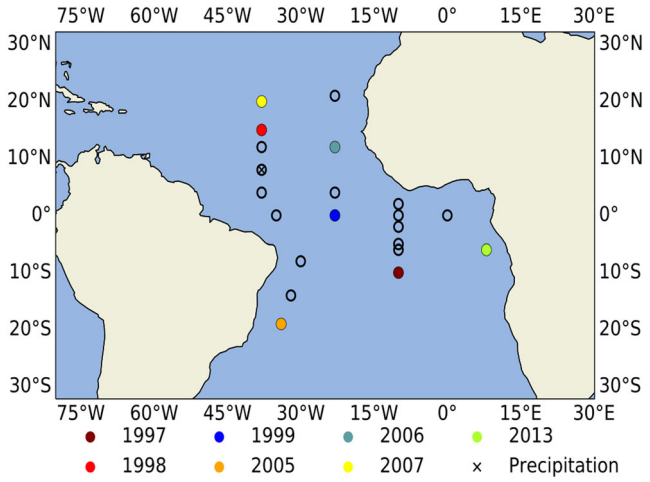

Figure 1. PIRATA mooring locations. Closed circles represent the moorings with pressure used in this study. Starting year for each record is color coded as shown in legend. Mooring where precipitation data is analyzed is shown with an "x."

numerical models, tending to suppress the build-up of convective available potential energy (CAPE; Dai & Trenberth, 2004). Moreover, in some atmospheric models (e.g., the atmospheric component of the Community Climate System Model 2), the convective-nonconvective precipitation ratio is too large (Dai & Trenberth, 2004). This triggers a surplus of deep convection, thereby prematurely removing moisture from the atmosphere (Dai & Trenberth, 2004). This results in a weak diurnal cycle of precipitation over the open ocean, particularly in the tropics where convection plays a large role in controlling precipitation initiation (Dai & Trenberth, 2004). Later models such as the Community Atmospheric Model (CAM) Versions 4 (CAM4) and 5 (CAM5) show a similar effect (Chen & Dai, 2019). Yin and Porporato (2017) investigated the efficiency with which the modeled diurnal cycle of clouds can reflect and absorb terrestrial radiation. It was concluded that there is an overestimation of radiation in models that could potentially lead to uncertainties in climate predictions. Also, the Coupled Model Intercomparison Project Phase 5 models either have an eastern or western Atlantic bias in the ITCZ location, while none of the models properly simulates precipitation (Siongco et al., 2015). Fortunately, there are some positive impact studies that suggest that newer models are representing clouds more realistically (see Stanfield et al., 2014, for more details).

This study seeks to improve our understanding of what drives the daily meridional wind anomaly pattern and open-ocean precipitation by examining for the first time the surface expression of the nonmigrating component of the atmospheric tides in the tropical Atlantic Ocean. We also extend the analysis of the migrating ATT's impact on zonal wind that was found in UD08. In contrast to the work done by UD08 in the tropical Pacific Ocean, where there was minimal land influence, in the tropical Atlantic the African continent may play a role in the dynamics of ATTs. Therefore, the unique aspects of this study are the analysis of surface tides in the tropical Atlantic using a combination of in situ data, satellite data, and a global reanalysis product to establish links between surface nonmigrating tides and the diurnal cycle of meridional winds and open-ocean precipitation. These results could have important implications for the representation of atmospheric thermal tides and their relationship to convection and precipitation in numerical models. In particular, they may aid in forecasting of surface heat, momentum, and fresh water fluxes over the open ocean, which could improve air-sea coupling.

This paper is arranged as follows: Section 2 describes the data sets and reanalysis product used in this study and details of the methodology. Section 3 examines the annual and seasonal influence of migrating and nonmigrating tides on surface pressure and wind fields and their associated linear momentum balance. The diurnal behavior of open-ocean precipitation in boreal summer is also discussed in section 3. Section 4 provides a summary, conclusions, and a discussion of how these results could be generalized in the future across the entire tropics.

2. Data and Methodology

2.1. Data

This section discusses the data sets and reanalysis products that are used to analyze surface atmospheric tides and their effects on precipitation in the tropical Atlantic. We use hourly measurements of surface atmospheric pressure, wind velocity, and rainfall from seven buoys of the Prediction and Research moored Array in the Tropical Atlantic (PIRATA; Bourlès et al., 2019). The locations of the buoys are shown in Figure 1. Measurements from the moorings on the equator and along 10°W, and between 4°N and 15°N along 38° W, began in 1997–1998, with various expansions added over time (Bourlès et al., 2019). Records from the other moorings in the North Atlantic began in 2006–2007 and from the moorings in the Southwest Atlantic in 2005. At 6°S, 8°E, regular data collection began in 2013 after an initial 1-year pilot deployment in 2006–2007. In this study, we are limited to analyzing data from the seven PIRATA moorings that measure atmospheric pressure (colored circles in Figure 1).

While PIRATA offers high-resolution in situ measurements in the open ocean, additional gridded data sets are required to provide an integrated basin-scale view. For this purpose, we use the second Modern-Era Retrospective analysis for Research and Applications (MERRA-2) global data set. It has a spatial resolution of 0.625° longitude by 0.5° latitude and an hourly temporal resolution. The MERRA-2 variables analyzed are surface barometric pressure and 10-meter zonal and meridional components of wind velocity. For robust statistics and analysis of MERRA-2 over a time period that overlaps with the majority of the PIRATA time series, we focus on the 20-year time period from 1998 to 2018. To ensure that results using MERRA-2 are robust, we also use the European Center for Medium-range Weather Forecasting's (ECMWF) ERA5 (ECMWF Re-Analysis) reanalysis data set. ERA5 has a similar spatial (0.625° × 0.5°) and temporal (hourly) grid as MERRA-2 and is analyzed over the same 20-year time period.

Since there are limited in situ precipitation measurements in the open ocean, the Integrated Multi-satellitE Retrievals for GPM (IMERG) satellite rainfall product is used. IMERG began collecting rainfall data in 2014, and for our analysis, we focus on the time period of 2014 to 2018. The data is half-hourly on a global 0.1° × 0.1° grid, which we spatially interpolate onto the MERRA-2 grid and average to hourly intervals to match MERRA-2. Because of the significant precipitation associated with the migrating ITCZ, hourly precipitation data from the 8°N, 38°W PIRATA mooring (denoted by x symbol in Figure 1) is also used for comparison to the hourly IMERG precipitation record.

Since IMERG is a fairly short data set, the Tropical Rainfall Measurement Mission (TRMM Version 7) was used to assess how well IMERG captures the features of precipitation in the tropical Atlantic. Our analysis of TRMM covers 10 years (2000–2010) of the 3-hourly data set.

2.2. Methodology

Much of our analysis is based on forming diurnal composites of PIRATA, MERRA-2, IMERG, and TRMM data. To examine whether the composites vary seasonally, the data are partitioned into December-January-February (DJF), March-April-May (MAM), June-July-August (JJA), and September-October-November (SON). Hourly diurnal composites are then calculated for each season and at each grid point (or mooring location) located within the tropical Atlantic region. For example, for the MERRA-2 diurnal composites during JJA, each of the 24 values of the diurnal composite at each grid point were calculated from 1911 individual values (21 years × 91 days per season). The significance of the hourly composites is determined via Student's two-tailed t test, which provides confidence intervals at the 95% level for each hour of each season. For JJA, the MERRA-2 confidence levels assume 1,911 independent values for each hour of the day.

To isolate the atmospheric tidal signal for each season, we use the methodology proposed by Sakazaki et al. (2015). We obtain the full atmospheric tidal field at each latitude by calculating the seasonal anomalies of pressure and winds at each grid point from the hourly composite. To compute the migrating component, we average the diurnal composites at the same local time globally across all 24 time zones (i.e., each average is performed along a characteristic curve in local hour and longitude space for each latitude). Once this is completed, the nonmigrating tide is calculated as the difference between full and migrating tidal components. This algorithm differs from the traditional zonal wavenumber spectra approach in that it provides a physical approach where an aggregate of a large (but finite) number of zonal wavenumbers are presented in physical space and not just one wavenumber at a time (Sakazaki et al., 2015).

Using the hourly full, migrating, and nonmigrating tidal fields, we then perform harmonic analysis on the diurnal composites. Since we are interested in the diurnal and semidiurnal harmonics, our equation to compute the amplitudes and phases is given by

$$F(x, y, t) = A_1\cos\left(\frac{2\pi t}{24}\right) + A_2\sin\left(\frac{2\pi t}{24}\right) + B_1\cos\left(\frac{2\pi t}{12}\right) + B_2\sin\left(\frac{2\pi t}{12}\right) + \text{Constant},$$

where A_1 and A_2 are the diurnal amplitudes, B_1 and B_2 are the semidiurnal amplitudes, and t is hour of the day. The phase is calculated as

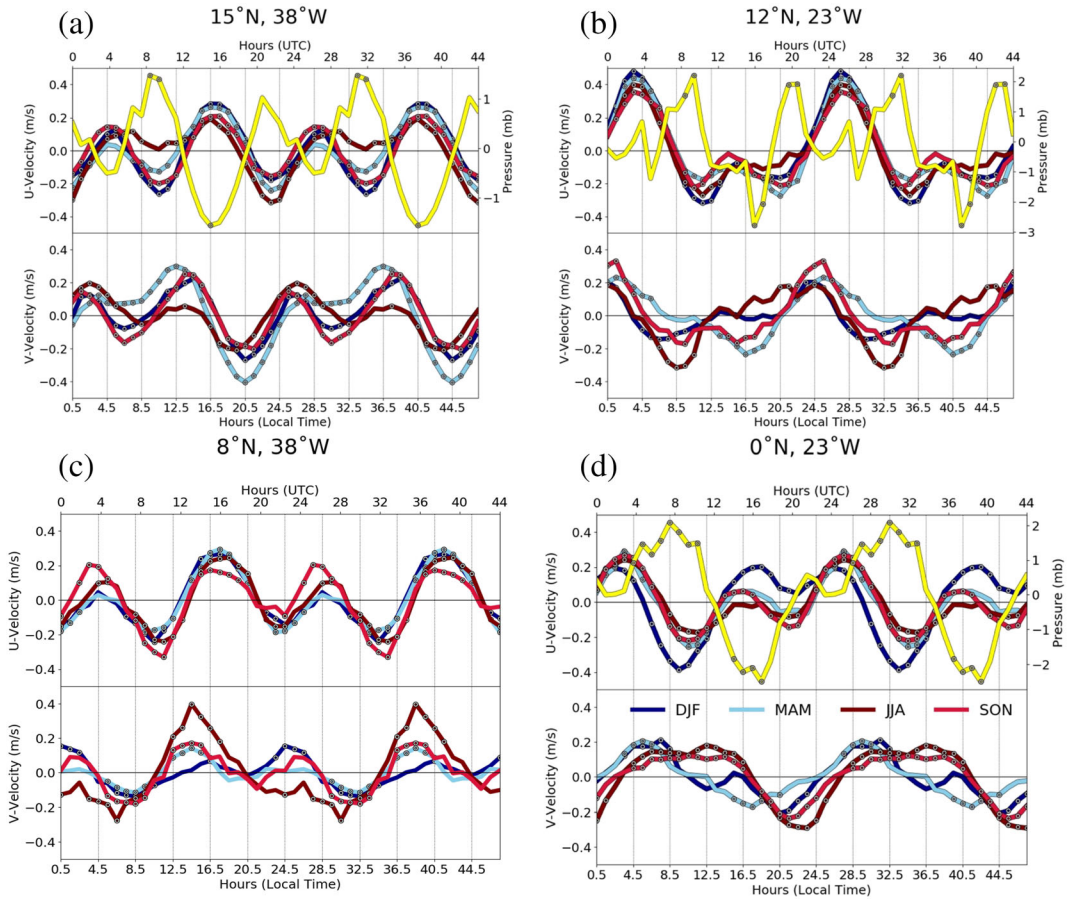

Figure 2. Diurnal composites of zonal (a, b) and meridional (c, d) wind anomalies (with respect to the daily average) at four PIRATA moorings along the 23°W line of longitude and the 38°W line of longitude composited for all seasons (DJF, MAM, JJA, and SON). Yellow lines show annual diurnal composites of surface pressure anomalies measured at the 15°N, 38°W; 12°N, 23°W; and 0°N, 23°W moorings. Circles indicate hourly values that are significant with 95% confidence determined from a two-tailed*t*test.

$$\theta_1 = \tan^{-1}\frac{A_2}{A_1}$$

for the diurnal phase, and

$$\theta_2 = \tan^{-1}\frac{B_2}{B_1}$$

for the semidiurnal phase.

3. Results

The diurnal composites of zonal winds from PIRATA moorings along 38°W and 23°W show a semidiurnal signal for all seasons and locations, consistent with migrating ATTs (upper panels in Figures 2a–2d). Maxima are present around hours of 03:30 and 16:30 and minima approximately at 10:30 and 21:30 local time. The PIRATA surface pressure annual composites at the three moorings where pressure data are available (yellow lines in Figures 2a, 2b, and 2d) show semidiurnal signals with 180° phase difference relative to zonal wind.

The meridional wind diurnal cycles (lower panels in Figures 2a–2d) have a stronger seasonal dependence and regional difference compared to the zonal wind. The 8°N, 38°W mooring (Figure 2c) shows the

strongest meridional winds, peaking at an average of 0.4 m s^{-1} at 14:30 LT for JJA. This timing could be due to the diurnal evolution of the marine boundary layer, which destabilizes during the day as a result of sensible heating at the surface. This allows for mixing of turbulent momentum within the marine boundary layer and thus an increase in wind speed during the afternoon (Dai & Deser, 1999). At most of the locations and for most seasons the meridional wind composites have a significant diurnal rather than a semidiurnal cycle. Similar diurnal variations in the meridional winds were reported in DS98 and UD08, but no complete explanation was given as to why they exhibit a diurnal cycle beyond advancing the hypothesis that the nonmigrating tides play a role. In this study, we seek to answer this question by investigating the nonmigrating component of ATTs and its relation to the diurnal cycle of meridional winds in the tropical Atlantic.

3.1. MERRA-2 Validation

Before investigating the basin-scale structure of the ATTs, we first validate diurnal composites generated from the MERRA-2 pressure and wind fields against those generated from PIRATA mooring observations. As an example, pressure, zonal wind, and meridional wind composites from PIRATA and MERRA-2 are compared as a function of hour (UTC) for the 0°, 23°W mooring during JJA (Figure 3). Here, the PIRATA and MERRA-2 diurnal composites of pressure (blue and red lines in Figure 3a, respectively) agree very well in terms of semidiurnal amplitude and phase, with relatively small residuals (black line in Figure 3a). Note that there is a difference in time between Figure 2 (local time) and Figure 3 (UTC), which makes the peak pressure signal appear shifted. MERRA-2 assimilates pressure data from PIRATA, so the good agreement between the pressure composites is expected. Somewhat larger discrepancies are found in the semidiurnal amplitude of zonal wind (Figure 3b) and to a lesser extent in the diurnal amplitude of meridional wind (Figure 3c), though there is fairly good agreement in the phasing of the zonal and meridional wind signals despite MERRA-2 not directly assimilating these fields. This location and season were chosen to illustrate some of the larger errors in amplitude and phase that can arise between PIRATA and MERRA-2. Other locations generally have much smaller errors.

While MERRA-2 seems to perform well at this location, an analysis is performed comparing the diurnal and semidiurnal amplitudes for each season to the ERA5 reanalysis to give an independent assessment of MERRA-2. Note that ERA5 also assimilates PIRATA pressure data. The seasonal RMS differences in surface pressure and winds between observations and MERRA-2 at the seven PIRATA locations with pressure data (Figure 1) are compared to the RMS differences between observations and ERA5 (not shown). Overall, MERRA-2 outperforms ERA5 for both diurnal and semidiurnal amplitudes and for all variables. For MERRA-2, the average RMS differences of diurnal amplitudes of surface pressure, u, and v are 0.085, 0.090, and 0.087, respectively, compared to 0.098, 0.138, and 0.102 for ERA5. For semidiurnal amplitudes the RMS differences are 0.074, 0.045, and 0.042 for MERRA-2 and 0.082, 0.065, and 0.058 for ERA5.

MERRA-2 fields are further validated by comparing the diurnal and semidiurnal amplitude ratios between the PIRATA and MERRA-2 pressure, zonal and meridional wind diurnal composites (Figures 4 and 5, respectively). These ratios were calculated for each of the seven mooring locations with pressure data (Figure 1) and for each season. An amplitude ratio greater (less) than unity indicates that MERRA-2 underestimates (overestimates) the PIRATA amplitude. Overall, there is good agreement for surface pressure, with a mean diurnal amplitude ratio of 1.16 (squares in Figure 4) and mean semidiurnal pressure amplitude ratio of 0.94 for all moorings and all seasons (squares in Figure 5). This indicates that MERRA-2 underestimates the PIRATA diurnal amplitude and overestimates the PIRATA semidiurnal amplitude. Since pressure is dominated by a semidiurnal signal (Figure 3a), the underestimation of the diurnal pressure amplitudes by MERRA-2 is less critical.

The zonal wind amplitude ratios are generally close to unity as well (circles in Figures 4 and 5), with diurnal and semidiurnal ratios ranging from 0.3–2.6 and 0.62–1.32, respectively. There is more seasonal and spatial dependence in the ratios for diurnal zonal wind amplitudes. For example, at 0°, 23°W MERRA-2 underestimates the PIRATA diurnal cycle for MAM, JJA, and SON by a factor 2 to 3, but the ratio is close to 1 in DJF (blue circles in Figure 4). In contrast, MERRA-2 overestimates the amplitude of the semidiurnal component by 18–38% during all seasons at this location (blue circles in Figure 5). The meridional winds perform similarly to the zonal wind amplitudes, with diurnal and semidiurnal ratios (diamonds in Figures 4 and 5) ranging from 0.15–6.5 (the largest value of 6.5 is for season JJA at 6°S, 8°E and is not shown) and 0.37–1.25, respectively. The large range of values is driven by the presence of outliers. For example, at 6°S, 8°E

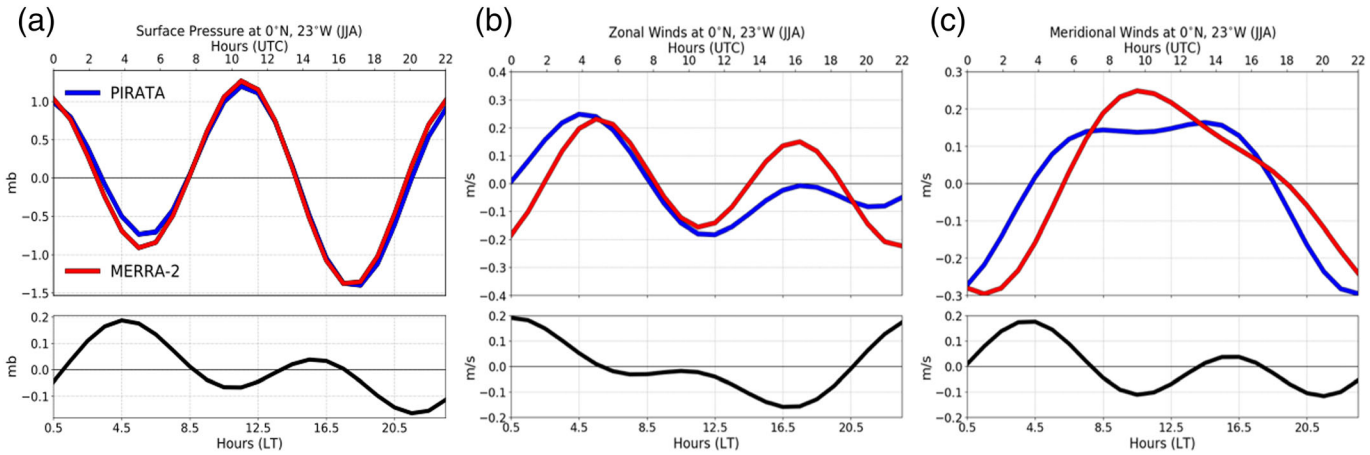

Figure 3. Comparisons of the fitted diurnal cycle from harmonic analysis of PIRATA (blue line) and MERRA-2 (red line) surface pressure (a), zonal wind speed (b), and meridional wind speed (c) anomalies at 0°N, 23°W for boreal summer (JJA). The top plots are the anomalies with respect to the daily mean and the bottom plots are the residual anomalies (PIRATA-MERRA-2).

MERRA-2 overestimates the semidiurnal amplitudes by up to 63% in JJA (yellow diamond in Figure 5c) while the diurnal amplitude ratios in the meridional wind for 6°S, 8°E during JJA (Figure 4c) are larger than 3 and therefore not shown.

While the ratio of the zonal and meridional wind velocity amplitudes may vary from mooring to mooring, the spatially and seasonally averaged zonal wind amplitude ratio for the diurnal and semidiurnal harmonics are close to unity (1.11 and 0.83, respectively). The ratios for the meridional wind diurnal and semidiurnal harmonics are similarly well represented (1.2 and 0.82, respectively). Standard deviations of the diurnal harmonic for pressure, zonal wind, and meridional wind are 0.2, 0.6, and 1.1, while the semidiurnal harmonic

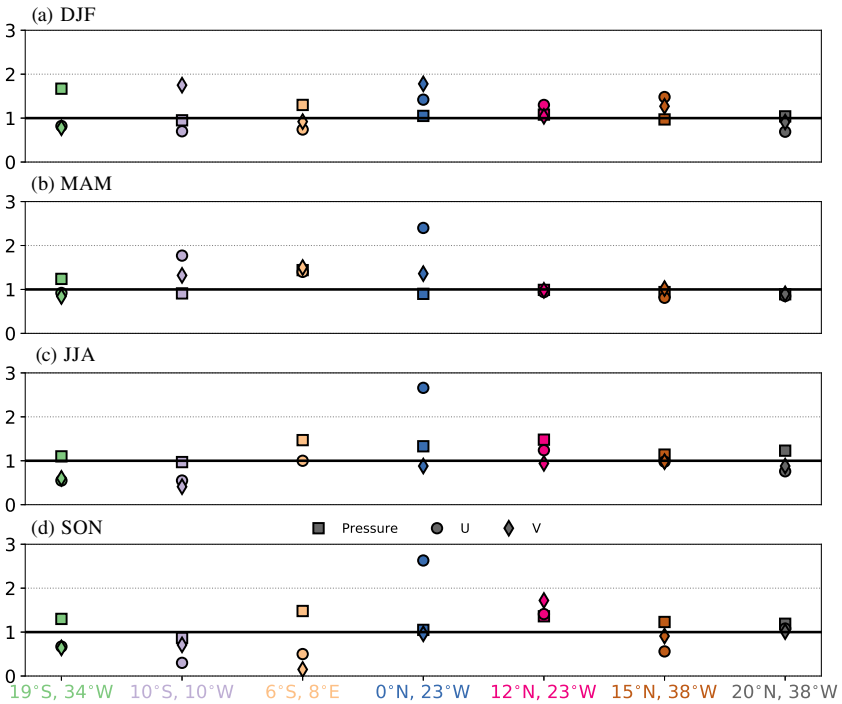

Figure 4. (a–d) Seasonal distribution of diurnal amplitude ratios of surface pressure (squares), u-wind (circles), and v-wind (diamonds) for PIRATA/MERRA-2 determined by harmonic analysis at the seven PIRATA moorings with pressure data (mooring latitude and longitude indicated on *x*axis).

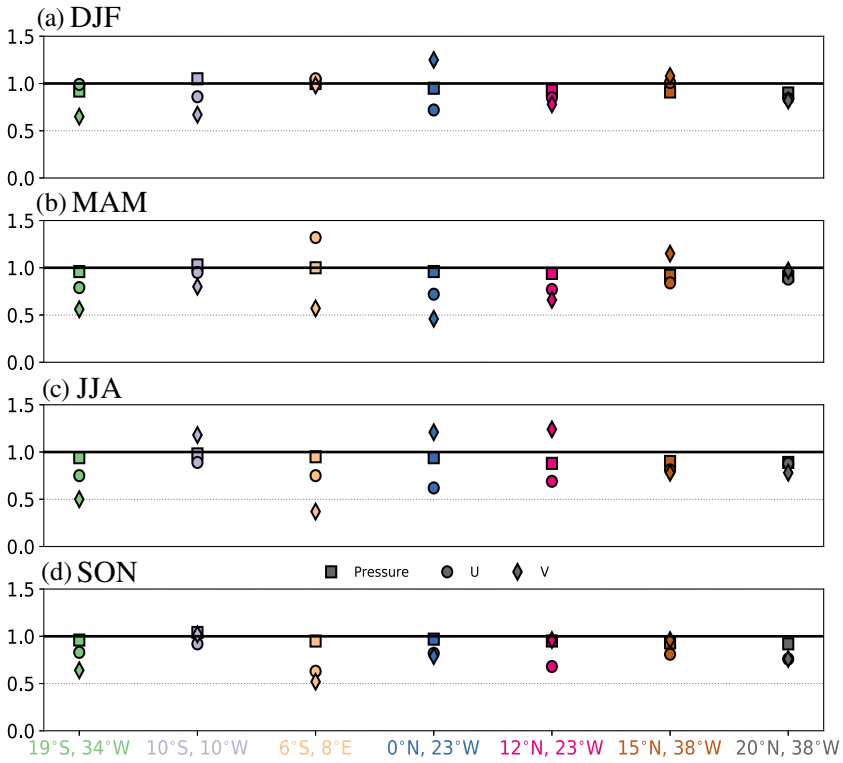

Figure 5. (a–d) Seasonal distribution of semidiurnal amplitude ratios of surface pressure (squares), u-wind (circles), and v-wind (diamonds) for PIRATA/MERRA-2 determined by harmonic analysis at the seven PIRATA moorings with pressure data (mooring latitude and longitude indicated on*x*axis).

has an overall smaller standard deviation for each variable (0.04, 0.14, and 0.25, respectively). Based on these comparisons with PIRATA and ERA5, it is concluded that MERRA-2 is a suitable data set to study ATT in the tropical Atlantic.

3.2. Atmospheric Thermal Tides From MERRA-2

Daily evolution of the full and migrating tides (see section 2.2) for DJF and JJA are examined for the hours 06:00 UTC (Figures 6a–6d) and 12:00 UTC (Figures 6e–6h). These seasons are chosen since they show the largest differences in spatial and temporal variations of the atmospheric tides. The full and migrating tides are primarily semidiurnal, and for brevity hours 18:00 and 24:00 are not shown since these hours are very similar to the hours 06:00 and 12:00, respectively. We also only show seasons DJF and JJA since they represent very different times of the year when the angles of the sun's insolation are exactly opposite.

For both seasons, the diurnal pressure variations present in the full tide (top panels in Figure 6) are largely captured by the migrating tide (bottom panels in Figure 6), with negative pressure anomalies over the ocean at hour 06:00 (Figures 6a–6d) and positive pressure anomalies over the ocean at hour 12:00 (Figures 6e–6h). The spatial locations of pressure extrema in the full tides vary between seasons, and this is also well represented by the spatial structure of the migrating tidal component (cf. comparisons at hour 06:00; Figures 6a–6d), with spatial correlations (Pearson's correlation coefficient; see Wilks, 1995, for more details) above 0.9. Despite this good agreement, compared to the migrating tides (bottom panels), the full tides (top panels) show a far more complex zonal and meridional structure associated with land effects on the pressure anomalies, likely due to strong diurnal air temperature fluctuations over land.

The wind patterns are shown for the full and migrating tides (black vectors on top of contours in Figure 6). Large differences are present between the tidal fields, especially over land. The migrating component of the winds has weaker amplitudes and a more uniform orientation throughout the domain compared to the full tides. The wind patterns shown in Figure 2 agree well with the patterns seen in Figure 6. For example, in Figures 2b and 2d there is an ~6-hr phase lag between the pressure (yellow line) and the zonal wind

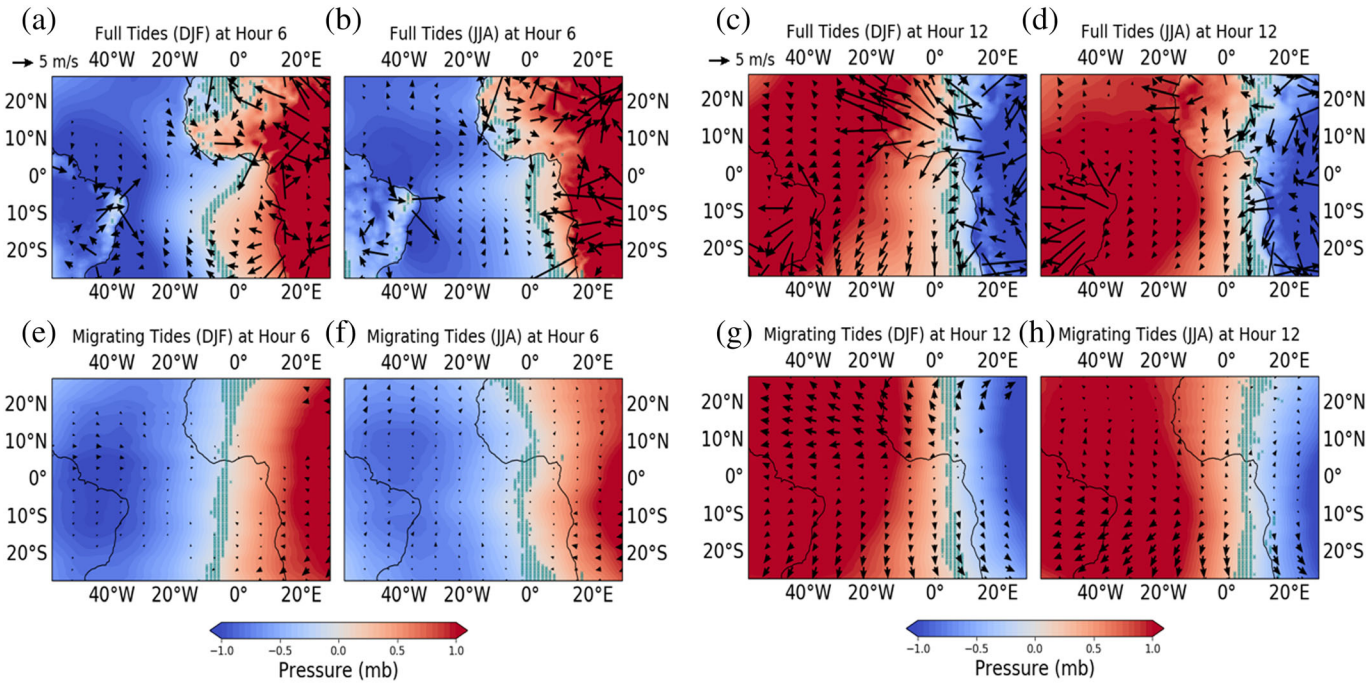

Figure 6. Latitude-longitude maps of full (a–d) and migrating atmospheric thermal tides (e–h) derived from MERRA-2 surface pressure for hours 06:00 and 12:00 UTC for the boreal winter (DJF) and summer (JJA) seasons. Wind vectors are overlaid to show the tidal u and v components for full tide (a–d) and migrating (e–h). Lack of significance of the pressure tide is shown with green stippling (every 7.5° × 3°), and significance of the wind speed is shown where arrows are present.

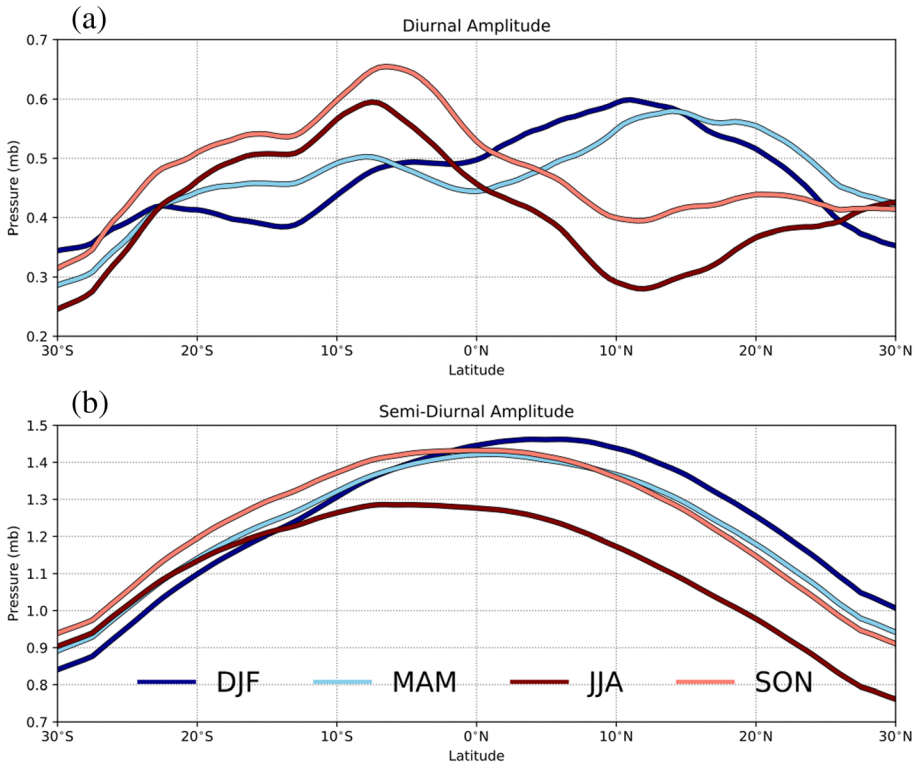

Figure 7. Seasonal distribution of MERRA-2 diurnal pressure amplitudes (a) and semidiurnal amplitudes (b) as a function of latitude for the migrating atmospheric thermal tide at 0°E.

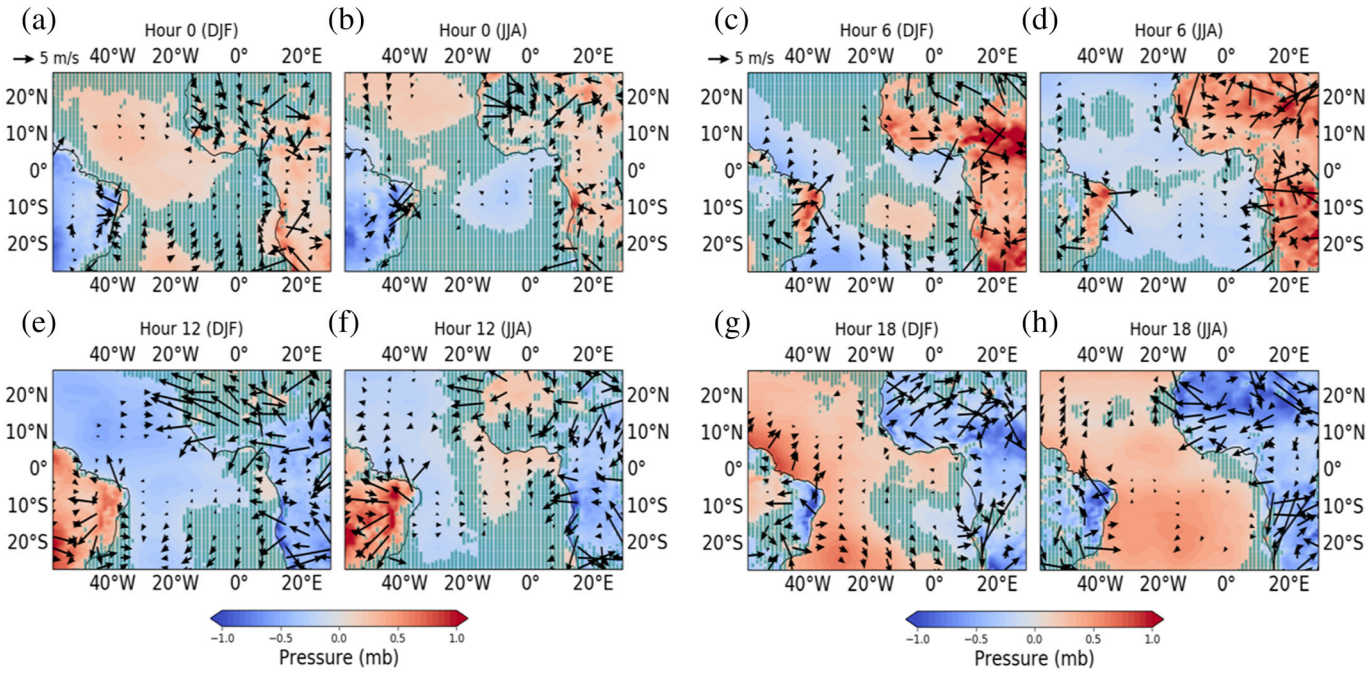

Figure 8. Latitude-longitude maps of nonmigrating atmospheric thermal tides derived from MERRA-2 surface pressure for hours 00:00 (a and b), 06:00 (c and d), 12:00 (e and f), and 18:00 (g and h) UTC for the boreal winter (DJF, left panels) and summer (JJA, right panels) seasons. Wind vectors are overlaid to show the tidal u and v components for full tide (a–d) and migrating (e–h). Lack of significance of the pressure tide is shown with green stippling (every 7.5° × 3°), and significance of the wind speed is shown where arrows are present.

response so that when the pressure anomaly is at a maximum, the mooring experiences easterly wind and vice versa. This is seen in the migrating plots at 12:00 UTC (Figures 6g and 6h). The maximum winds follow the latitudinally shifted maximum pressure anomaly seen at hour 12:00 UTC for DJF (at 10°N in Figure 6g) and JJA (10°S in Figure 6h).

In general, the diurnal and semidiurnal amplitudes of the migrating pressure tides have largest amplitudes near the tropics and decrease in strength toward higher latitudes (Figure 7). However, the hemisphere in which maximum diurnal amplitudes are found changes seasonally, consistent with the hemispheric shifts in the seasonal maximum absorption of solar radiation, with a maximum near 6–8°S in JJA and SON (orange and brown lines in Figure 7a) and near 10°N in DJF and MAM (light and dark blue lines in Figure 7a). The semidiurnal amplitudes show a maximum near the equator for MAM and SON, a peak in the Northern Hemisphere for DJF, and a peak in the Southern Hemisphere for JJA (Figure 7b). Overall, the semidiurnal amplitudes are twice as large as those for the diurnal harmonic, consistent with DS98 and UD08.

The pressure amplitudes associated with the nonmigrating tides (Figure 8) are typically smaller compared to their migrating tidal counterparts (Figure 6, bottom panels). The nonmigrating tides also have a stationary diurnal oscillation over the ocean throughout the day, consistent with UD08 findings in the tropical Pacific. However, we observe a phase difference in the nonmigrating pressure anomalies over land versus the ocean. Despite being generally weaker, the nonmigrating component is an important component of the full tide, especially over land, where larger pressure anomalies occur due to stronger diurnal temperature anomalies, which could be enhanced by vegetation and orography. As mentioned in the introduction, the associated convective updrafts over land contribute to nonmigrating tides by latent heat release (Hendon & Woodberry, 1993). Wind patterns for the nonmigrating tides show a much more chaotic picture than the migrating counterpart. The strongest amplitudes of the winds occur over land (Figure 8), consistent with the large wind amplitudes seen in the full tides (Figure 6, top panels).

While it is well accepted that the migrating tide contributes to the zonal wind anomaly pattern in the tropical Pacific (e.g., DS98; Hagan & Forbes, 2003; UD08), much less is known about the relationship between the

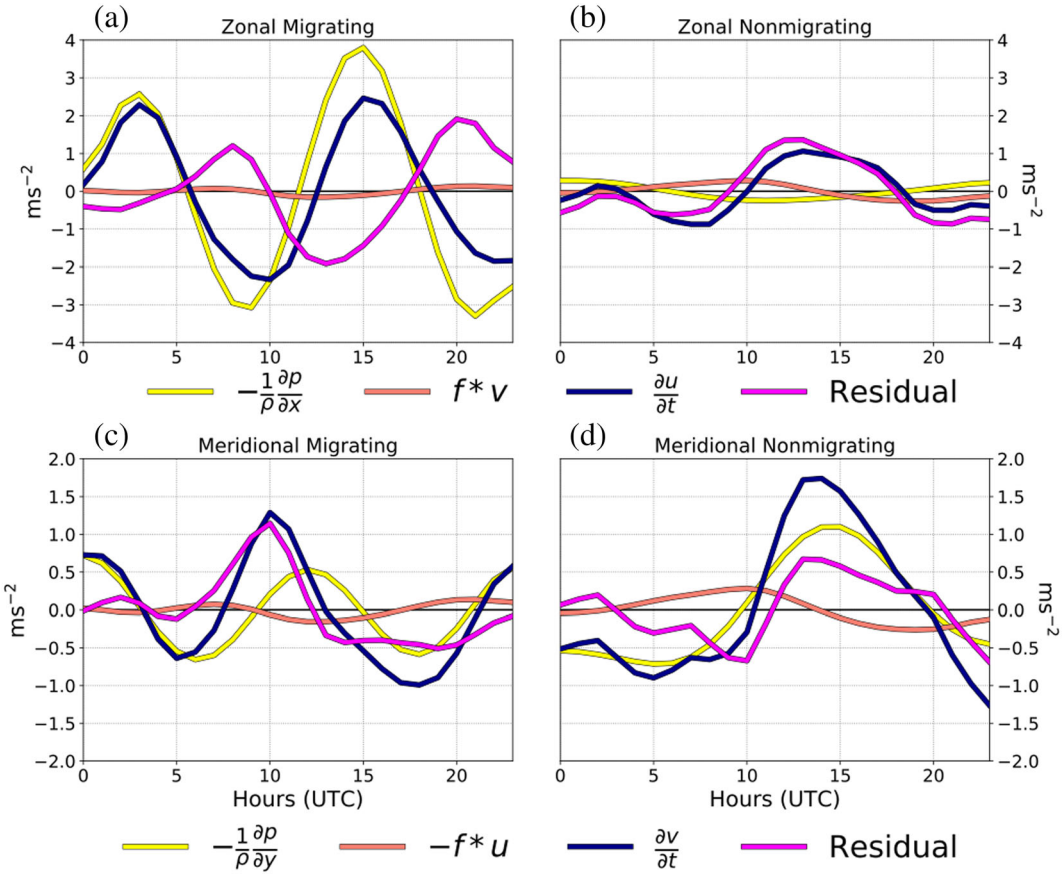

Figure 9. Annually averaged diurnal composites of MERRA-2 linear momentum terms ($\times 10^{-5}$) for the migrating component of the zonal wind tidal field (a), the nonmigrating component of the zonal wind tidal field (b), the migrating component of the meridional wind tidal field (c), and the nonmigrating component of the meridional wind tidal field (e) for an area average over the region 40–30°W and 5–8°N.

meridional winds and nonmigrating tides. UD08 computed the annually averaged amplitudes and phases of the diurnal harmonics for the linear meridional momentum equation from diurnal meridional pressure gradient harmonics used in Dai and Wang (1999) to show good agreement with observed meridional winds in the tropical Pacific Ocean. This suggests that there may be a link between the diurnal harmonic of the meridional pressure gradient (i.e., nonmigrating tide) and the daily cycle of meridional wind variability. To determine whether this link exists in the tropical Atlantic, the next two sections present analyses aimed at showing how the pressure gradient, acceleration, and Coriolis terms interact for the migrating and nonmigrating components of the zonal and meridional tides in MERRA-2.

3.3. Linear Momentum Terms Between 30°W and 40°W

To understand the dynamics driving the dominant tidal variations in the open ocean, we examine the annually averaged linear terms in the momentum budget within an offshore boxed region covering 40–30°W and 5–8°N. This region is chosen due to the presence of enhanced diurnal cycles of rainfall during the boreal summer months. In the following sections we make the case that the observed significant diurnal rainfall patterns are partially in response to convective processes over the African continent via the nonmigrating meridional wind field. Analysis near the West African coast in section 3.4 highlights this phenomenon.

In this box, we focus on the migrating component of the zonal wind tidal field (Figure 9a), the nonmigrating component of the zonal wind tidal field (Figure 9b), the migrating component of the meridional wind tidal field (Figure 9c), and the nonmigrating component of the meridional wind tidal field (Figure 9d). Note that

this region is chosen for consistency with the region in which open-ocean precipitation and divergence analysis is performed later in section 3.5. The momentum budgets in other locations in the tropical Atlantic have been similarly analyzed (not shown), including locations close to land, and the results show similar magnitudes and phases of the momentum budget terms.

For the zonal momentum budget of the migrating tide, the semidiurnal acceleration term (dark blue curve in Figure 9a) has a similar amplitude and phase as the zonal pressure gradient term (yellow curve in Figure 9a). The Coriolis term (salmon curve in Figure 9a) is nonzero but fairly small, so the balance in this open-ocean region is primarily between the acceleration, zonal pressure gradient, and residual (magenta curve in Figure 9a) terms. These residuals have maxima at roughly 8:00 and 20:00 UTC and appear to dampen the pressure-induced winds based on the phasing of the acceleration term. It is unclear what is driving this signal. It is possible that linear (or nonlinear) surface drag is playing a role, which would increase the residual and oppose the acceleration term.

The zonal nonmigrating term shows a diurnal cycle in the acceleration and residual terms (dark blue and magenta curves, respectively, in Figure 9b), with similar amplitudes and phases. There is a slightly larger Coriolis term (salmon curve in Figure 9b) compared to the zonal migrating Coriolis term (salmon curves in Figure 9a) but a much weaker pressure gradient term (yellow curves in Figure 9b). Overall, however, the magnitudes of the zonal nonmigrating terms (Figure 9b) are small compared to the zonal migrating terms (Figure 9a).

The acceleration and residual terms follow a similar semidiurnal pattern for the meridional migrating term (dark blue and magenta curves, respectively, in Figure 9c). The maxima and minima in the meridional acceleration term (dark blue curve in Figure 9c) lead the zonal migrating acceleration (dark blue curve in Figure 9a) by 5–6 hr and are roughly half the magnitude. Interestingly, while the zonal migrating acceleration (dark blue curve in Figure 9a) experiences similar phasing as the pressure gradient term (yellow curve in Figure 9a), there is a slight offset in maxima between the acceleration and pressure gradient for the meridional migrating term (dark blue and yellow curves, respectively, in Figure 9c), with the acceleration leading the pressure gradient term during daylight hours.

The nonmigrating meridional momentum balance differs from the nonmigrating zonal momentum balance, with forcing from the meridional pressure gradient term (yellow curve in Figure 9d) in phase with the large amplitude acceleration term (dark blue curve). The Coriolis term shows a slight diurnal periodicity (salmon curve in Figure 9d) but is still fairly small. In UD08, they concluded that the meridional pressure gradient term played an important role in the diurnal cycle of the meridional wind patterns in the tropical Pacific (as opposed to nonlinear factors) based on comparisons of observed meridional wind harmonics and phases and pressure-derived meridional wind harmonics from the Comprehensive Ocean-Atmosphere Data Set (see Dai & Wang, 1999, for more details). In contrast, here we also find large residuals (magenta curve in Figure 9d) in the nonmigrating momentum balance, suggesting other nonlinear factors contribute to acceleration of the meridional winds. However, since the pressure gradient is in phase with the acceleration term and has a similar magnitude, it appears that the nonmigrating pressure tide is largely responsible for driving the diurnal meridional wind pattern in this region.

Overall, the momentum balance in the boxed region shows a few important details. The zonal migrating acceleration term seems to be driven by the pressure gradient, and the acceleration for the zonal migrating balance is much larger than the zonal nonmigrating counterpart. This corroborates what has been found in previous literature (e.g., DS98 and UD08). Conversely, the meridional nonmigrating acceleration appears to be driven by the meridional nonmigrating pressure gradient and is also larger than the meridional migrating acceleration term. Therefore, this analysis provides evidence that the nonmigrating tide drives the meridional wind diurnal cycle in this open ocean region.

3.4. Linear Momentum Terms Across the Tropical Atlantic

To better understand the latitudinal dependence of the momentum budgets across the tropical Atlantic, and whether the results from section 3.3 can be generalized, we consider zonally averaged annual mean diurnal and semidiurnal amplitudes of the linear momentum equation terms, including the residual. Here we assume that the accumulated errors from the combined linear terms are small and that the residual term is dominated by contributions from nonlinear momentum budget terms. Because the migrating tide is

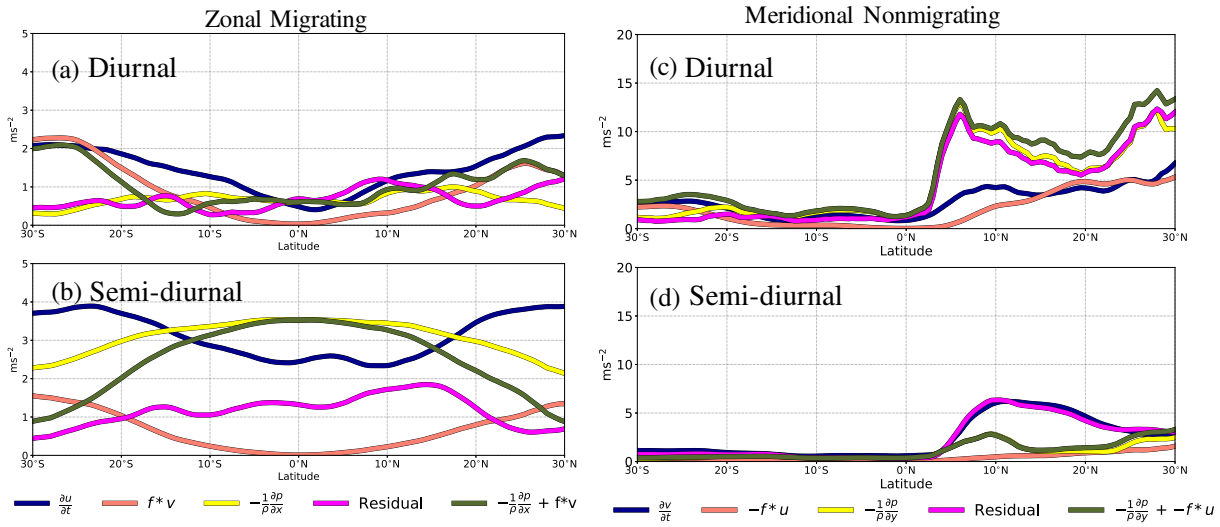

Figure 10. Latitudinal dependence of the zonally averaged amplitudes averaged over all seasons of the MERRA-2 migrating (a, b) and nonmigrating (c, d) linear momentum terms. Due to the lack of zonal dependence across time zones, 0° is shown for the migrating terms while a zonal average from 0–20°W is shown for the nonmigrating terms. Note that the *y*axis of the right panels (nonmigrating terms) is 4 times larger than the *y*axis of the left panels (migrating terms).

zonally independent, the amplitudes shown in Figures 10a and 10b are along longitude 0°. However, since the nonmigrating tides are zonally dependent we show the tides averaged between 0°E and 20°W (Figures 10c and 10d) to see what effect the West African landmass has on the nonmigrating momentum balance over surrounding waters. As mentioned in section 3.3, the West African landmass provides is a source of nonmigrating tides that impact the meridional wind field (shown in this section), which may influence the diurnal cycle of surface divergence/convergence and precipitation (shown in section 3.5).

Since we are broadening the scope of the momentum balance analysis from an area-averaged region in the central tropical North Atlantic in section 3.3, here we look at a larger latitudinal range to examine processes across the latitudinal extent of the tropical Atlantic (Figure 10). We only show the zonal migrating momentum terms and the meridional nonmigrating momentum terms, as they are the dominant terms for each wind component, respectively (Figure 9). The diurnal amplitudes of the migrating component of zonal momentum terms show that the acceleration (dark blue line in Figure 10a) and Coriolis (salmon line in Figure 10a) terms are smallest at the equator and increase poleward, whereas the diurnal amplitude of

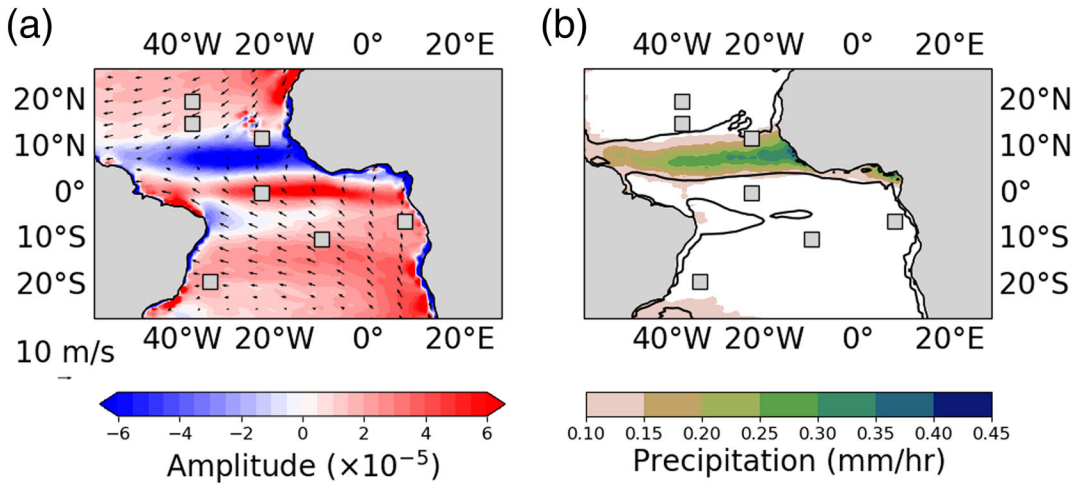

Figure 11. Seasonal averages of (a) wind velocity divergence (shaded) and wind velocity (vectors) and (b) precipitation. The black contour in panel (b) represents the zero contour of wind divergence, indicating the region of convergence. All PIRATA mooring locations are shaded gray in (a) and (b).

the zonal pressure gradient term does not vary dramatically with latitude and remains relatively small (yellow line Figure 10a). Poleward of about 15° latitude, the amplitude of the residual term (magenta line in Figure 10a) is small compared to the dominant terms in the momentum balance. In contrast, equatorward of ±15° the residual term becomes comparable in magnitude to the individual momentum balance terms.

The semidiurnal cycle shows largest zonal pressure gradient term amplitudes in the tropics while the acceleration term amplitudes are largest toward midlatitudes (yellow and dark blue lines, respectively, in Figure 10b). The semidiurnal amplitude of the residual term (magenta line in Figure 10b) is generally smaller than the other terms but is larger than Coriolis (salmon line in Figure 10b) equatorward of ±20°. Acceleration (dark blue line in Figure 10b) is largely driven by the zonal pressure gradient term from 15°S to 15°N and depends more heavily on the Coriolis term (salmon line in Figure 10b) outside of that latitudinal band. This highlights the important role of the zonal pressure gradient in driving the migrating zonal winds for the semidiurnal harmonic in the tropics.

A strong spike in the diurnal amplitudes of the meridional pressure gradient and residual terms occurs around 5°N in the diurnal amplitudes of the nonmigrating meridional momentum balance (yellow, green, and magenta lines, respectively, in Figure 10c), with relatively high values poleward of the spike. This large amplitude in the pressure gradient term and residual term is related to the land-ocean difference in the nonmigrating tides (as seen in Figure 8), which drives strong pressure gradients and accelerations. In contrast to the pressure gradient term and residual, the diurnal amplitudes of the Coriolis and acceleration terms increase gradually north of 5°N (salmon and dark blue lines, respectively, in Figure 10c). The sharp spike in the amplitude of the residual, combined with an absence of a spike in amplitude in the acceleration and Coriolis terms, suggests that the nonlinear terms of the momentum equations become abruptly important over land and that the pressure gradient is balancing the residual. The semidiurnal amplitudes of the nonmigrating meridional momentum terms show relatively small amplitudes for all terms compared to the diurnal amplitudes but also exhibit an abrupt increase in the amplitudes of the meridional acceleration and residual terms near 5°N again pointing to the importance of the nonlinear terms (dark blue and magenta lines, respectively, in Figure 10d).

Overall, the momentum budget analysis confirms that for the semidiurnal zonal migrating tides the zonal pressure gradient term controls acceleration in the tropics, consistent with UD08 and others (e.g., Haurwitz & Cowley, 1973). Poleward of 20°, diurnal and semidiurnal contributions from the Coriolis term become more important for the zonal migrating tides; however, we are primarily concerned with the tropical region in this study where Coriolis remains relatively weak. The nonmigrating momentum terms show a much more complex structure, but overall the pressure gradient and residual terms are stronger over land and near the coasts (north of 5°N) and weaker over the open ocean (south of 5°N). Note that the y axis for Figures 10c and 10d is 4 times that of Figures 10a and 10b, which indicates the importance of the nonmigrating terms relative to the migrating terms north of 5°N. The sharp spikes in the momentum terms over land may be associated with strong diurnal temperature anomalies over the land, which could lead to diabatic heating and convection over the course of a daily cycle. This convection over land could potentially enhance the morning peak of daily precipitation in the open ocean (Sato et al., 2009). Preliminary analysis shows that nonlinear terms associated with land effects (not included in the linear momentum balance) contribute to the large residual term amplitudes, specifically vertical advection of momentum (not shown). Properly accounting for these nonlinear advection terms as well as linear (or nonlinear) friction terms in the momentum budget should reduce the amplitude of the residuals, but it is beyond the scope of the work presented here.

3.5. Impacts of Nonmigrating Tides on Open-Ocean Precipitation

To investigate the possible impact of meridional nonmigrating tides on precipitation in the open ocean, we consider the connection between surface convergence associated with convection over Africa and offshore precipitation from the IMERG and TRMM data sets. The seasonally averaged surface divergence of the wind velocity for JJA shows a strong band of convergence from about 5°N to 11°N, marking the seasonal mean location of the ITCZ (blue shading in Figure 11a). This zonally banded region of enhanced surface convergence is driven primarily by the meridionally converging northeasterly and southeasterly trade winds in the western/middle portions of the basin and southwesterly winds near the western Africa coast (vectors in Figure 11a). Enhanced seasonally averaged precipitation from IMERG (color shading in Figure 11b)

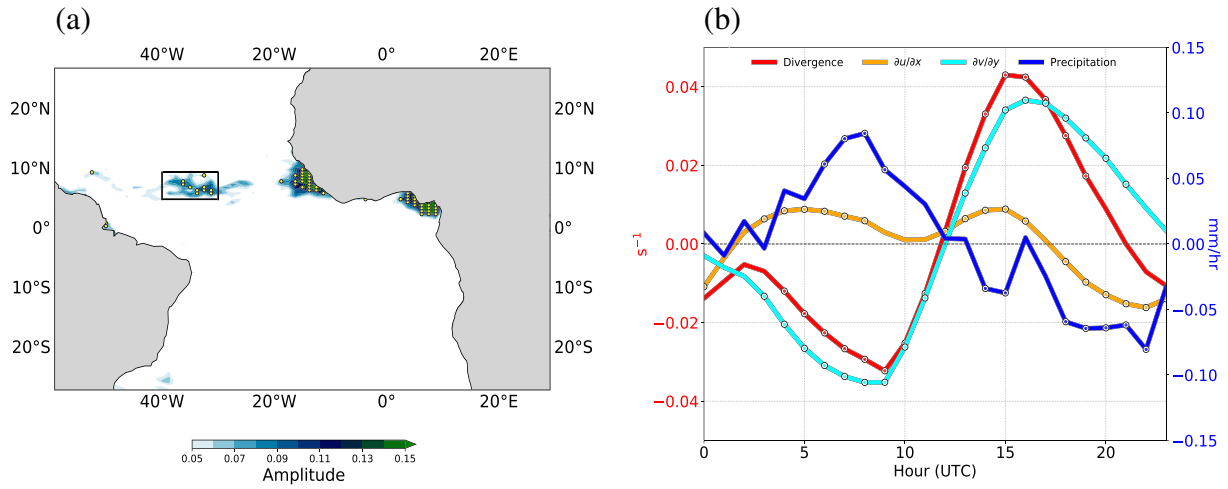

Figure 12. Diurnal amplitude of precipitation in (a) with a threshold of 0.05 mm/hr in JJA. Area-averaged hourly composites (b) of anomalies with respect to the daily mean for precipitation, divergence, zonal, and meridional components of the divergence for the boxed region in (a) during JJA. The yellow dots in (a) indicate locations where the amplitude of the diurnal cycle is significant at the 95% confidence level. The circles in (b) indicate significance within the 95% confidence interval.

overlaps with the band of convergence, based on the zeroth-divergence line (black contour in Figure 11b). JJA is chosen due to the robustness of open-ocean precipitation diurnal amplitudes associated with the close proximity of the ITCZ during the summer.

Diurnal precipitation amplitudes for JJA (shading in Figure 12a) are shown across the entire tropical Atlantic. The yellow dots indicate locations where the amplitude of the diurnal cycle is significant at the 95% confidence level. This is determined by analyzing the significance of each hour of the seasonal composites (at each location) using a Student's *t* test. If over a diurnal period there exist at least 2 hr with significant diurnal precipitation maxima (significantly different than 0) that are followed by 2 hr with significant minima (less than 0), that diurnal cycle amplitude is considered significant. This is a somewhat subjective way to determine the significance of the diurnal amplitudes, but it is likely a conservative approach given the strict criteria. Other seasons were analyzed in a similar fashion (not shown) but did not show significant diurnal amplitudes for much of the open ocean, including this boxed region.

Near 7°N, 35°W, in the middle of the ITCZ, we find a cluster of enhanced and significant diurnal amplitudes of open-ocean precipitation (boxed region in Figure 12a). Area averages of diurnal composites of precipitation, total wind velocity divergence, and the zonal and meridional components of wind velocity divergence in this boxed region as a function of time in hours UTC show that the maximum precipitation in the morning (blue line in Figure 12b) corresponds well to the time of strongest negative divergence or convergence (i.e., anomalous convergence; red line in Figure 12b). Conversely, during times where the divergence is most positive in the afternoon, the precipitation rates are lower. This implies that there is a possible control of elevated precipitation rates by wind velocity convergence on diurnal time scales in this region for JJA. It is important to note that the meridional component of the divergence (cyan line in Figure 12b) appears to dominate the total divergence, illustrating the importance of the meridional winds in this region. The precipitation, total divergence, and meridional divergence curves exhibit primarily diurnal rather than semidiurnal variability, whereas the zonal divergence curve (yellow line in Figure 12b) varies semidiurnally. Combined with the results described in the earlier sections, this suggests that the diurnal nonmigrating tide, which drives the meridional wind variability, has a stronger influence on offshore diurnal precipitation in the ITCZ than the migrating semidiurnal tide, which drives the zonal wind variability.

Hovmöller plots of the nonmigrating divergence (Figure 13a) and its meridional component (Figure 13b) along 7°N, near the center of the boxed region in Figure 12, again show that the meridional component dominates the total divergence field for each season. There is wave-like westward propagation of the diurnal divergence and convergence signals for DJF and MAM (Figure 13a). Strong convergence occurs around

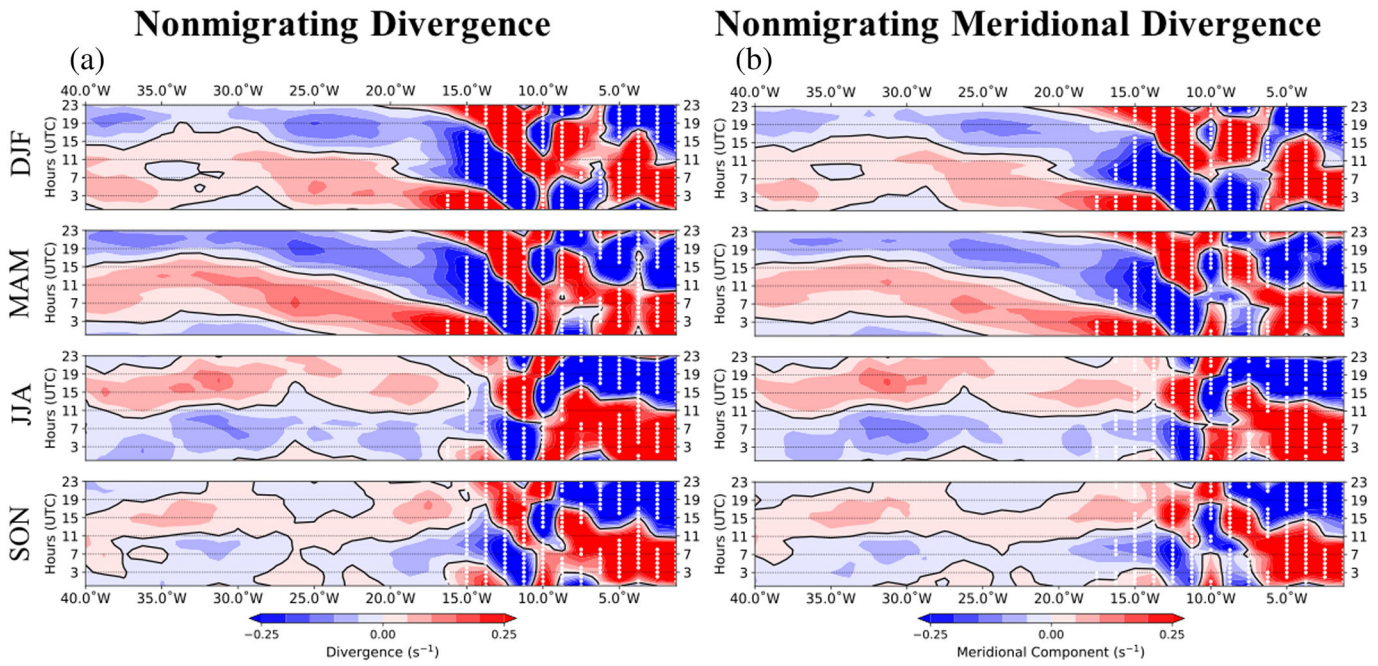

Figure 13. Hovmöller diagrams, with longitude as the abscissa and time (UTC) on the ordinate axis, for the divergence (a) and $\frac{\partial v}{\partial y}$ (b). The domain stretches from 40°W to 0°E along 7°N, which overlaps with the box region in Figure 12a. White dots represent the points that are significant at the 95% confidence level.

00:00 UTC at 12°W and may initiate convergence over the open ocean, however much of the signal lacks significance west of 16°W. During JJA and SON (third and fourth panels in Figures 13a and 13b), the convergence over land occurs at around 20:00–11:00 UTC near 12°W and 15:00 near 15°W to 24:00 near 20°W, which extends nearly instantaneously over the open ocean from 20°W to 40°W and persists through the early morning hours. While not highly significant, this extended region from ~15–40°W shows maximum convergence around 09:00 UTC at 32°W, consistent with the timing of convergence noted in Figure 12b.

A similar diurnal pattern in the tropical North Atlantic off the west coast of Africa during JJA has been documented before in the literature (see Dai & Deser, 1999; Yang & Slingo, 2001). It is thought that gravity waves carry land-based signals of brightness temperature (i.e., clouds and implied precipitation) to open-ocean regions (Yang & Slingo, 2001). It was hypothesized that these signals are contributing factors to precipitation patterns found in offshore regions. It is possible that these signals are due to convectively coupled westward propagating inertia-gravity waves or mixed Rossby-gravity waves, though more detailed analysis would be needed for a determination of which waves are involved.

As noted earlier, the DJF divergence signal shows strong convergence associated with convection initiating around 00:00 UTC at 12°W and propagating to 32°W in 24 hr (Figure 13a). This puts the propagation speed of the wave at roughly 25–26 m/s, similar to what was observed in the Bay of Bengal (Yang & Slingo, 2001). During JJA, we see a zonal band of the convergence/divergence signal that is possibly driven by convective processes over land (Figure 13c), similar to that of DJF and MAM. The nearly immediate response over the open ocean is potentially due in part to the westward propagating African Easterly Jet, which peaks in boreal summer at 7°N (Nicholson & Grist, 2003), and would increase the westward wave propagation speed. It is also possible that local oceanic effects play a role in surface convergence/divergence over the open ocean.

Based on the combination of the Hovmöller diagrams of nonmigrating divergence (Figure 13), area-averaged divergence, and enhanced area-averaged precipitation rates (Figure 12a), in JJA in the central ITCZ there appears to be a coherent signal between the surface wind convergence in the morning, driven by nonmigrating tides, and the early morning maximum of precipitation. To provide an independent validation of the area-averaged IMERG precipitation rate anomalies in JJA (blue line), we compute direct diurnal composites constructed from PIRATA rainfall observations at 8°N, 38°W for the same season (red line in Figure 14) and

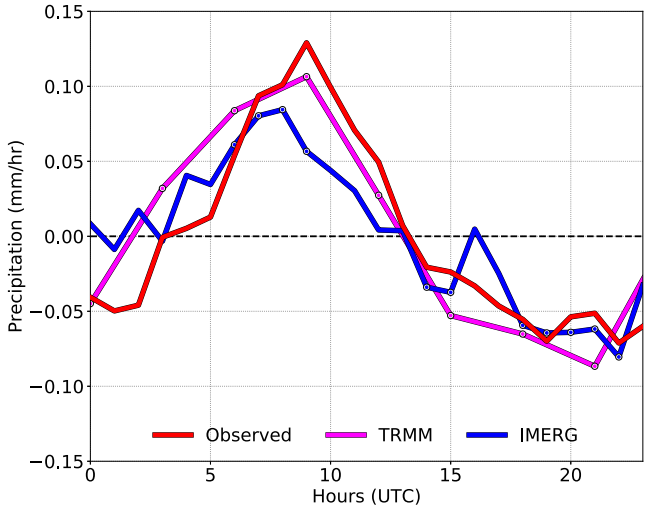

Figure 14. Hourly composites of IMERG area-averaged precipitation rates (blue), TRMM area-averaged precipitation rates (magenta), and PIRATA observations (red) at 8°N, 38°W for JJA. Circles show when hourly IMERG and TRMM values are significant with 95% confidence based on a two-tailed*t*test.

using historical data (2000–2010) from TRMM. There is good agreement in the timing and amplitude of peak precipitation in the early morning between 08:00 and 09:00 UTC and in the timing of the minimum precipitation in the afternoon/evening hours for all three independent data sets. However, the IMERG area-averaged composite appears to lead the PIRATA composite by an hour, perhaps due to the zonal range of the box (30°W to 40°W), lying mostly eastward of the mooring longitude (38°W). TRMM, however, appears to capture the correct phase of maximum rainfall. Due to the noisy nature of point observations of the PIRATA rainfall measurements, the significance of the PIRATA diurnal composite is not assessed here, though over 1,000 observations per hour are included in this calculation (92 days per season and more than 10 years of measurements) which means that differences between the two curves may not be significant.

4. Summary and Discussion

This study analyzed the diurnal and semidiurnal evolution of zonal and meridional winds from PIRATA moorings along 38°W and 23°W and investigated the physical drivers of the observed variations. The link between the semidiurnal zonal wind pattern and migrating atmospheric tides that was documented in DS98 and UD08 provided a platform to study the nonmigrating tides' impact on the meridional wind diurnal cycle. The migrating and nonmigrating components of the atmospheric thermal tides were examined to determine the extent to which each component aids in driving the wind pattern and the potential link to open-ocean precipitation.

For calculating the migrating and nonmigrating components of the atmospheric thermal tides, we used a global reanalysis product, MERRA-2. To quantify how well the data set performs compared to observations, a harmonic analysis was performed to obtain diurnal and semidiurnal amplitudes of pressure, zonal wind, and meridional wind tidal fields, which are then used to compute ratios (PIRATA/MERRA-2) for each harmonic. While some discrepancies between MERRA-2 and PIRATA exist, the differences are generally small, as most locations and seasons compared well for all the variables. Thus, MERRA-2 fields can be used to understand how atmospheric tides control daily pressure and wind variations across the tropical Atlantic.

A linear momentum balance analysis was then performed to determine which terms drive the migrating and nonmigrating tidal winds. Overall, the annually averaged zonal migrating terms averaged over an open ocean region from 40–30°W and 5–8°N show an approximate balance between the acceleration and pressure gradient terms. However, there are also significant maxima in the residual term at 08:00 and 20:00 UTC. This elucidates times when the nonlinear terms, such as the vertical momentum flux divergence in the marine boundary layer, play an important role. The nonmigrating zonal terms are relatively small but show the acceleration and residual terms in phase with a weak diurnal cycle. The meridional migrating term shows semidiurnal cycles in the acceleration and the residual terms that lead the zonal migrating acceleration by 5–6 hr. The meridional nonmigrating momentum balance shows strong amplitudes in the acceleration, pressure gradient, and residual terms, with a maximum at 13:00–15:00 UTC.

The zonal migrating diurnal amplitudes along 0°E are small within the tropical band (20°S to 20°N) while the semidiurnal amplitudes of the zonal migrating pressure gradient and pressure gradient plus Coriolis peak at the equator. The zonally averaged nonmigrating meridional field has a strong spike in the meridional pressure gradient, sum of pressure gradient and Coriolis, and residual terms around 5°N, near the start of the African continent. Overall, the nonmigrating momentum terms were larger than the migrating terms north of 5°N. These results indicate that nonlinear terms become important in the equations of motion over land, perhaps due to advective-convective processes. This has been corroborated by preliminary analysis of the vertical advection term over the tropical Atlantic (not shown), which indicates that vertical advection remains much weaker compared to the linear terms over the open ocean. However, over coastal regions the vertical advection strengthens and plays a more prominent role in the momentum balance.

Dai and Deser (1999) looked at semidiurnal and diurnal wind patterns over the globe and found that land regions (particularly near coastlines) experience maximum divergence at local dawn, while maximum divergence over the ocean occurs during evening hours. Our work shows a similar result, with a dipole of divergence between land and ocean. Figure 13 shows maximum divergence over land (10–15°W) starting at approximately 08:00 UTC and persisting throughout the day for all seasons. During boreal winter and spring, the wind velocity convergence/divergence signal moves offshore (15–40°W) in the late evening hours in a wave-like pattern. During the boreal summer, there is strong convergence initiating at 20:00–11:00 UTC at 12°W and 15:00–24:00 UTC from 15–20°W. A zonal band of convergence propagates nearly instantaneously from 20°W to 40°W starting from 00:00 UTC and persisting throughout the morning hours. It is thought that evening convective processes over the African continent contribute to this convergence signal.

The explanation of the divergence signal presented in Dai and Deser (1999) is consistent with ours, namely that temperatures rapidly increase over land areas during the daytime hours and cool more quickly than the ocean during the evening, creating large land-ocean temperature differences. This results in a large-scale circulation in which surface air rises and converges over the African continent and sinks and diverges over the ocean in the evening hours.

Significant diurnal cycles of precipitation and convergence were only observed in the open-ocean region of the ITCZ in boreal summer. The meridional winds in the ocean were found to be forced in part by nighttime convection over land and driven by the nonmigrating tides, which affect the convergence and divergence patterns found in the open ocean. It was also shown that these diurnal convergence patterns in JJA are associated with significant early morning open-ocean precipitation diurnal cycles and follow nighttime convection over land. Direct measurements of precipitation from a PIRATA mooring agree quite well with area-averaged satellite precipitation rates and therefore align well with the diurnal cycle of divergence noted above.

This work is the first to propose the importance of the nonmigrating tides in the early-morning precipitation maximum in offshore regions of the tropical Atlantic. Schematically, the sun rises in the morning, heating the continental regions and lowering the surface pressure in the evening hours. This causes an increase in the surface convergence, which can initiate convection and drive strong nonmigrating tidal signals. We hypothesize that the meridional convergence signal is then translated to offshore regions via the nonmigrating component of the atmospheric tide, aided by the African easterly jet in JJA. This enhances convergence over the open ocean in early morning, which we claim leads to the increase in diurnal precipitation rates.

Proper representation of the diurnal cycle of precipitation in general is difficult to capture in global models (Dai, 2006; Dai & Trenberth, 2004; Sato et al., 2009) since convective-scale processes are usually handled with parameterizations. Resolving these issues requires an increase in horizontal and vertical resolution or higher-dimensional cloud-resolving models, which comes at the cost of computational time (Sato et al., 2009).

This study may help to address these issues by providing observational evidence of open-ocean rainfall produced by convection over land potentially being driven by nonmigrating tides. There are a few ways this is helpful: First, the tidal decomposition used in this study can be used to examine the realism of how nonmigrating tides are represented in the model by season. This would be important for capturing the diurnal cycles correctly (per season) and would provide insight in how well convection is resolved over land. Second, corroboration of rainfall rates for JJA in the vicinity of the ITCZ from IMERG and the 8°N, 38°W PIRATA mooring helps to validate the IMERG data set as a useful tool for model diurnal rainfall validation. Lastly, the link between early morning meridional surface convergence driven by nonmigrating tides originating from land-based convection and open-ocean rainfall during JJA should be explored within a numerical model framework and could help identify ways to improve convection parameterizations.

More work needs to be done to generalize the results presented here. Applying this analysis to all three tropical observing systems is an important natural extension of this research. Specifically, it will be important to revisit earlier analyses of the TAO network in the tropical Pacific as well as examine data from the Research moored Array for African-Asian-Australian Monsoon Analysis and prediction (RAMA) in the tropical Indian Ocean.

Data Availability Statement

PIRATA data can be found at the NOAA Pacific Marine Environmental Laboratory website (https://www.pmel.noaa.gov/gtmba/pirata). MERRA-2 data can be found at NASA's Global Modeling and Assimilation Office website (https://gmao.gsfc.nasa.gov/reanalysis/MERRA-2/). The ERA5 data set is found on the ECMWF's website (https://www.ecmwf.int/). IMERG data can be found at NASA's Precipitation Measurement Missions website (https://pmm.nasa.gov/data-access/downloads/gpm). TRMM data can be found at NASA's Goddard Earth Sciences Data and Information Services Center website (https://disc.gsfc.nasa.gov/; https://doi.org/10.5067/TRMM/TMPA/3H/7).

Acknowledgments

J. A. C. was supported in part under the auspices of the Cooperative Institute for Marine and Atmospheric Studies (CIMAS), a cooperative institute of the University of Miami and NOAA, cooperative agreement NA20OAR4320472. The authors were supported by NOAA's Ocean Global Ocean Monitoring and Observing (GOMO) program (Funding Reference 100007298) and the Atlantic Oceanographic and Meteorological Laboratory (AOML). This research was performed while the author held an NRC Research Associateship award at the Naval Research Laboratory. The authors would like to thank all the reviewers and to Hosmay Lopez for their insightful comments and suggestions.

Reference

Bain, C. L., Magnusdottir, G., Smyth, P., & Stern, H. (2010). Diurnal cycle of the Intertropical Convergence Zone in the east Pacific. *Journal of Geophysical Research*, *115*, D23116. https://doi.org/10.1029/2010JD014835

Bourlès, B., Araujo, M., McPhaden, M. J., Brandt, P., Foltz, G. R., Lumpkin, R., et al. (2019). PIRATA: A sustained observing system for tropical Atlantic climate research and forecasting. *Earth and Space Science*, *6*, 577–616. https://doi.org/10.1029/2018EA000428

Butler, S. T., & Small, K. A. (1963). The excitation of atmospheric oscillations. *Proceedings of the Royal Society of London A*, *274*(1356), 91–121. https://doi.org/10.1098/rspa.1963.0116

Chapman, S., & Lindzen, R. S. (1970). *Atmospheric Tides*. D. Dordrecht: Holland: Reidel Press.

Chen, D., & Dai, A. (2019). Precipitation characteristics in the Community Atmosphere Model and their dependence on model physics and resolution. *Journal of Advances in Modeling Earth Systems*, *11*, 2352–2374. https://doi.org/10.1029/2018MS001536

Covey, C., Dai, A., Marsh, D., & Lindzen, R. S. (2011). The surface-pressure signature of atmospheric tides in modern climate models. *Journal of the Atmospheric Sciences*, *68*, 495–514. https://doi.org/10.1175/2010JAS3560.1

Dai, A. (2006). Precipitation characteristics in eighteen coupled climate models. *Journal of Climate*, *19*, 4605–4630. https://doi.org/10.1175/JCLI3884.1

Dai, A., & Deser, C. (1999). Diurnal and semidiurnal variations in global surface wind and divergence fields. *Journal of Geophysical Research*, *104*(D24), 31,109–31,125. https://doi.org/10.1029/1999JD900927

Dai, A., & Trenberth, K. E. (2004). The diurnal cycle and its depiction in the community climate system model. *Journal of Climate*, *17*, 930–951. https://doi.org/10.1175/1520-0442(2004)017<0930:TDCAID>2.0.CO;2

Dai, A., & Wang, J. (1999). Diurnal and semidiurnal tides in global surface pressure fields. *Journal of the Atmospheric Sciences*, *56*, 3874–3891. https://doi.org/10.1175/1520-0469(1999)056<3874:DASTIG>2.0.CO;2

Deser, C. (1994). Daily surface wind variations over the equatorial Pacific Ocean. *Journal of Geophysical Research*, *99*(D11), 23,071–23,078. https://doi.org/10.1029/94JD02155

Deser, C., & Smith, C. A. (1998). Diurnal and semidiurnal variations of the surface wind field over the tropical Pacific Ocean. *Journal of Climate*, *11*, 1730–1748. https://doi.org/10.1175/1520-0442(1998)011<1730:DASVOT>2.0.CO;2

Garreaud, R. D., & Wallace, J. M. (1997). The diurnal march of convective cloudiness over the Americas. *Monthly Weather Review*, *125*, 3157–3171. https://doi.org/10.1175/1520-0493(1997)125<3157:tdmocc>2.0.co;2

Gray, W. M., & Jacobson, R. W. (1977). Diurnal variation of deep cumulus convection. *Monthly Weather Review*, *105*, 1171–1188. https://doi.org/10.1175/1520-0493(1977)105<1171:dvodcc>2.0.co;2

Hagan, M. E., & Forbes, J. M. (2003). Migrating and nonmigrating diurnal tides in the middle and upper atmosphere excited by tropospheric tides. *Journal of Geophysical Research*, *108*(A2), 1062–1076. https://doi.org/10.1029/2002JA009466

Hagan, M. E., & Robel, R. G. (2001). Modeling diurnal tidal variability with the National Center for Atmospheric Research thermosphere-ionosphere-mesosphere-electrodynamics general circulation model. *Journal of Geophysical Research*, *106*(A11), 24,869–24,882. https://doi.org/10.1029/2001JA000057

Hamilton, K. (1981). Latent heat release as a possible forcing mechanism for atmospheric tides. *Monthly Weather Review*, *109*(1), 3–17. https://doi.org/10.1175/1520-0493(1981)109<0003:LHRAAP>2.0.CO;2

Haurwitz, B., & Cowley, A. D. (1973). The diurnal and semidiurnal barometric oscillations, global distribution and annual variation. *Pure and Applied Geophysics*, *102*, 193–222. https://doi.org/10.1007/BF00876607

Hendon, H. H., & Woodberry, K. (1993). The diurnal cycle of tropical convection. *Journal of Geophysical Research*, *98*(D9), 16,623–16,637. https://doi.org/10.1029/93JD00525

Hsu, H. H., & Hoskins, B. J. (1989). Tidal fluctuations as seen in ECMWF data. *Quarterly Journal of the Royal Meteorological Society*, *115*, 247–264. https://doi.org/10.1002/qj.49711548603

Kousky, V. E. (1980). Diurnal rainfall variation in northeast Brazil. *Monthly Weather Review*, *108*, 488–498. https://doi.org/10.1175/1520-0493(1980)108<0488:DRVINB>2.0.CO;2

Kraus, E. B. (1963). The diurnal precipitation change over the sea. *Journal of the Atmospheric Sciences*, *20*, 546–551.

Lavoie, R. L. (1963). Some aspects of the meteorology of the tropical Pacific viewed from an atoll. *Atoll Research Bulletin*, *96*, 1–80. https://doi.org/10.5479/si.00775630.96.1

Lu, X., Liu, H.-L., Liu, A. Z., Yue, J., McInerney, J. M., & Li, Z. (2012). Momentum budget of the migrating diurnal tide in the Whole Atmosphere Community Climate Model at vernal equinox. *Journal of Geophysical Research*, *117*, D07112. https://doi.org/10.1029/2011JD017089

Nicholson, S. E., & Grist, J. P. (2003). The seasonal evolution of the atmospheric circulation over West Africa and equatorial Africa. *Journal of Climate*, *16*, 1013–1030. https://doi.org/10.1175/1520-0442(2003)016<1013:TSEOTA>2.0.CO;2

Sakazaki, T., & Hamilton, K. (2017). Physical processes controlling the tide in the tropical lower atmosphere investigated using a comprehensive numerical model. *Journal of the Atmospheric Sciences*, *74*, 2467–2487. https://doi.org/10.1175/JAS-D-17-0080.1

Sakazaki, T., Sato, K., Kawatani, Y., & Watanabe, S. (2015). Three-dimensional structures of tropical nonmigrating tides in a high-vertical-resolution general circulation model. *Journal of Geophysical Research: Atmospheres*, *120*, 1759–1775. https://doi.org/10.1002/2014JD022464

Sato, T., Miura, H., Satoh, M., Takayabu, Y. N., & Wang, Y. (2009). Diurnal cycle of precipitation in the tropics simulated in a global cloud-resolving model. *Journal of Climate*, *22*, 4809–4826. https://doi.org/10.1175/2009JCLI2890.1

Siongco, A. C., Hohenegger, C., & Stevens, B. (2015). The Atlantic ITCZ bias in CMIP5 models. *Climate Dynamics*, *45*, 1168–1180. https://doi.org/10.1007/s00382-014-2366-3

Stanfield, R. E., Dong, X., Xi, B., Kennedy, A., Del Genio, A. D., Minnis, P., & Jiang, J. H. (2014). Assessment of NASA GISS CMIP5 and Post-CMIP5 simulated clouds and TOA radiation budgets using satellite observations. Part I: Cloud fraction and properties. *Journal of Climate*, *27*, 4189–4208. https://doi.org/10.1175/JCLI-D-13-00558.1

Sui, C.-H., Li, X., & Lau, K.-M. (1998). Radiative–convective processes in simulated diurnal variations of tropical oceanic convection. *Journal of the Atmospheric Sciences*, *55*, 2345–2357. https://doi.org/10.1175/1520-0469(1998)055<2345:RCPISD>2.0.CO;2

Tao, W.-K., Lang, S., Simpson, J., Sui, C.-H., Ferrier, B., & Chou, M.-D. (1996). Mechanisms of cloud-radiation interaction in the tropics and midlatitudes. *Journal of the Atmospheric Sciences*, *53*(18), 2624–2651. https://doi.org/10.1175/1520-0469(1996)053<2624:MOCRII>2.0.CO;2

Ueyama, R., & Deser, C. (2008). A climatology of diurnal and semidiurnal surface wind variations over the tropical Pacific Ocean based on the tropical atmosphere ocean moored buoy array. *Journal of Climate*, *21*(4), 593–607. https://doi.org/10.1175/JCLI1666.1

Wallace, J. M., & Hartranft, F. R. (1969). Diurnal wind variations: Surface to 30 kilometers. *Monthly Weather Review*, *97*(6), 446–455. https://doi.org/10.1175/1520-0493(1969)097<0446:DWVSTK>2.3.CO;2

Wilks, D. S. (1995). *Statistical methods in the atmospheric sciences: An introduction*, *International Geophysics Series* (Vol. 59). San Diego: Academic Press.

Yang, G.-Y., & Slingo, J. (2001). The diurnal cycle in the tropics. *Monthly Weather Review*, *129*(4), 784–801. https://doi.org/10.1175/1520-0493(2001)129<0784:TDCITT>2.0.CO;2

Yin, J., & Porporato, A. (2017). Diurnal cloud cycle biases in climate models. *Nature Communications*, *8*, 2269. https://doi.org/10.1038/s41467-017-02369-4